

Supplementary Information

One-Pot Alkaline Vapor Oxidation Synthesis and Electrocatalytic Activity towards Glucose Oxidation of CuO Nanobelt Arrays

Tetsuro Soejima,^{*a,b} Hitomi Yagyu,^a Nobuo Kimizuka,^{b,c} and Seishiro Ito^a

^a Department of Applied Chemistry, School of Science and Engineering, Kinki University,
3-4-1 Kowakae, Higashi-osaka, Osaka 577-8502, Japan.

^b CREST, Japan Science and Technology Agency, 744 Moto-oka, Nishi-ku, Fukuoka 819-0395, Japan.

^c Department of Chemistry and Biochemistry, Graduate School of Engineering, Kyushu University,
744 Moto-oka, Nishi-ku, Fukuoka 819-0395, Japan.

*E-mail: soejima@apch.kindai.ac.jp

Experimental details

Characterization.

Field-emission scanning electron microscopy (SEM) was performed using Hitachi S-4800 type II (accelerating voltage, 10 kV). X-ray diffraction (XRD) was performed using Rigaku RINT 2500 using Cu K α radiation. ICP-AES measurement was performed using SHIMADZU ICP-7500.

Electrochemical Measurements.

Electrochemical measurements were performed on an HZ-5000 with HAG-1512m (HOKUTO DENKO). All electrochemical experiments were carried out using a conventional three-electrode system consisting of an Ag/AgCl (saturated KCl) reference electrode, a platinum wire counter electrode, and a CuO nanobelt arrays/Cu electrode (formation conditions; 100 mM NH₃–100 mM H₂O₂ aqueous solution, 80 °C, 7h). A 0.5 mol L⁻¹ NaOG aqueous solution was used as the supporting electrolyte. The electrolyte was stirring during the electrochemical measurement using a magnetic stirrer and a stirring bar.

Fig. S1

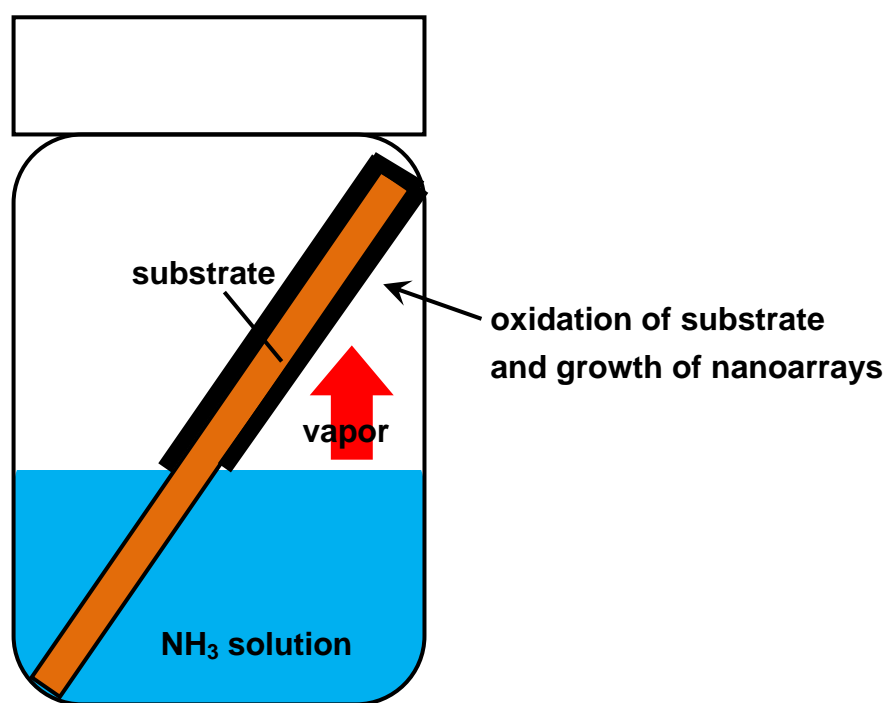


Fig. S1 The schematic illustration of a vapor oxidation (VO) growth process.

Fig. S2

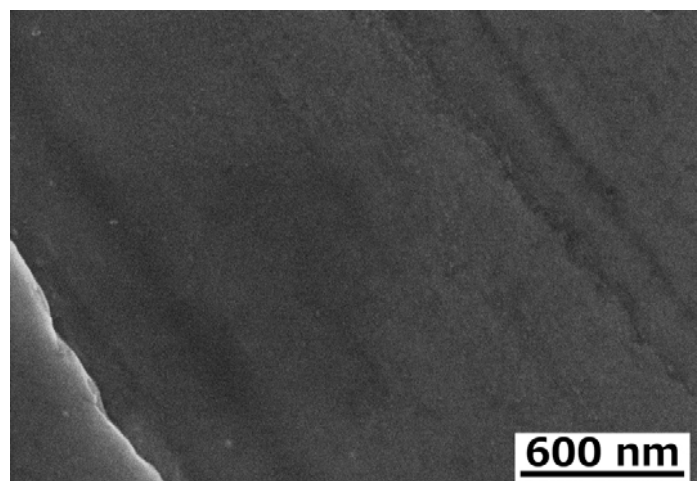


Fig. S2 An SEM image of Cu plate before the VO reaction.

Fig. S3

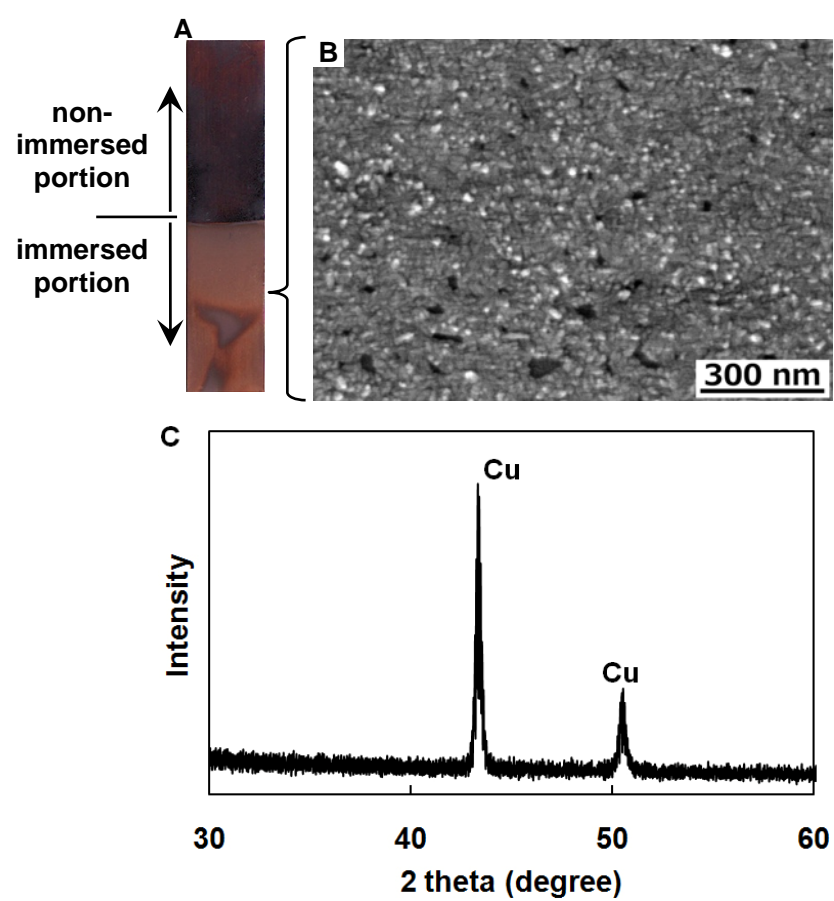


Fig. S3 (A) A Picture of a Cu plate after the VO reaction (100 mM NH₃–100 mM H₂O₂ aqueous solution). An SEM image (B) and XRD pattern (C) of Cu plate at the immersed portion.

Fig. S4

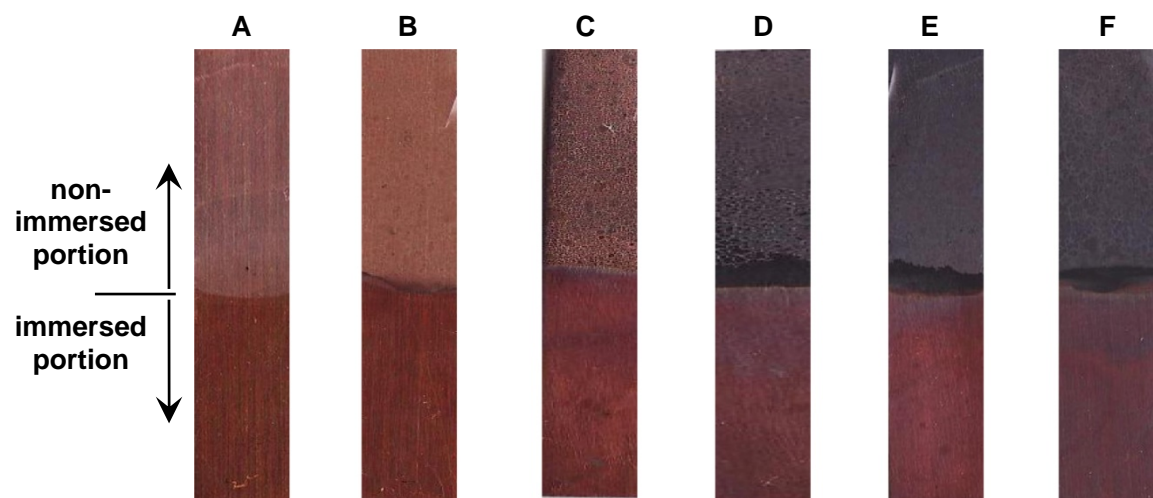


Fig. S4 Pictures of Cu substrates after the VO reaction: (A), 10min; (B), 30min; (C), 1h; (D), 3h; (E), 7h; (F), 10h.

100 mM NH₃–100 mM H₂O₂ aqueous solution (19 mL); reaction temperature, 80 °C.

Fig. S5

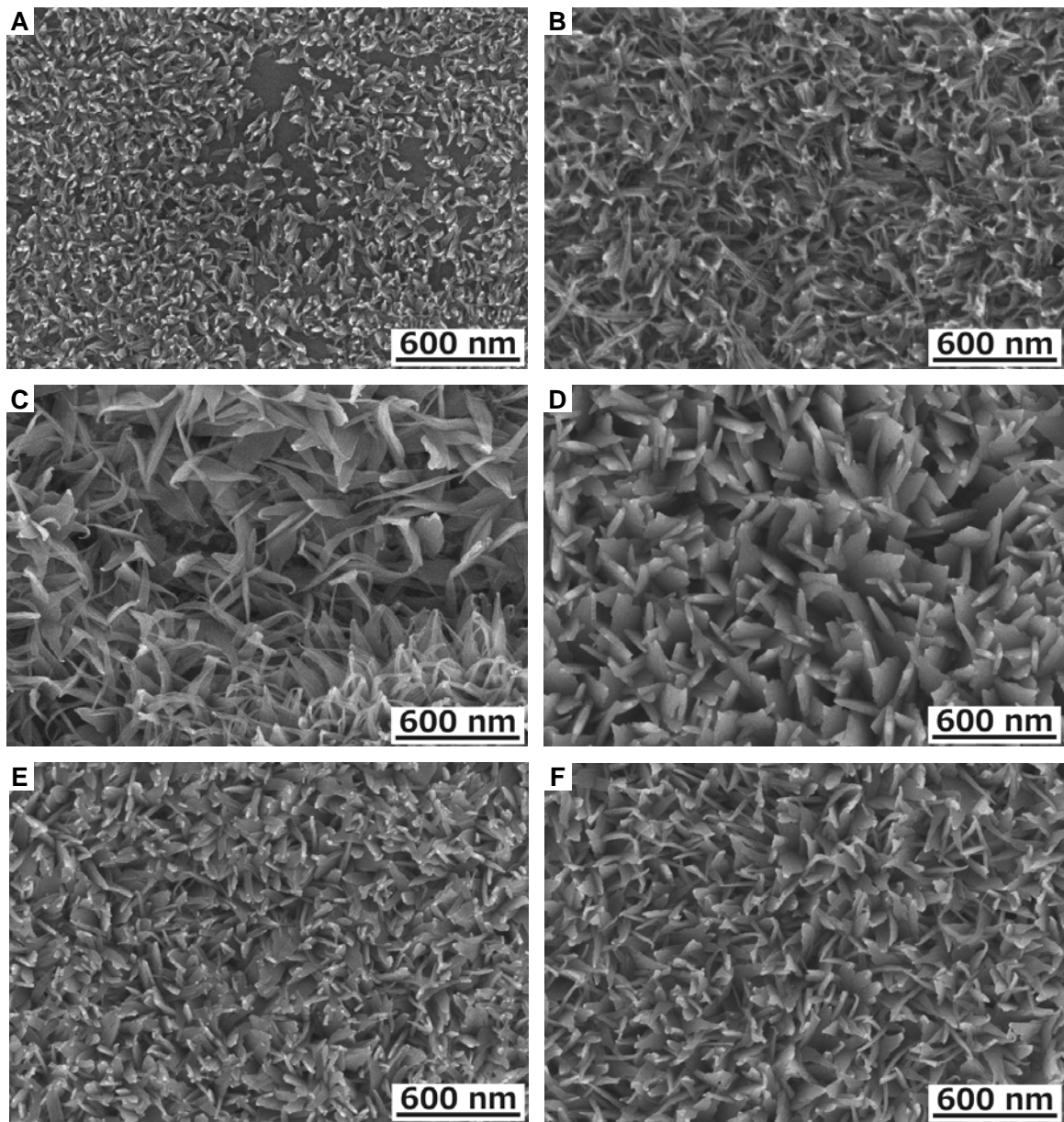


Fig. S5 SEM images of CuO nanobelt arrays obtained at varied reaction periods: (A), 10min; (B), 30min; (C), 1h; (D), 3h; (E), 7h; (F), 10h. 100 mM NH₃–100 mM H₂O₂ aqueous solution (19 mL); reaction temperature, 80 °C.

Fig. S6

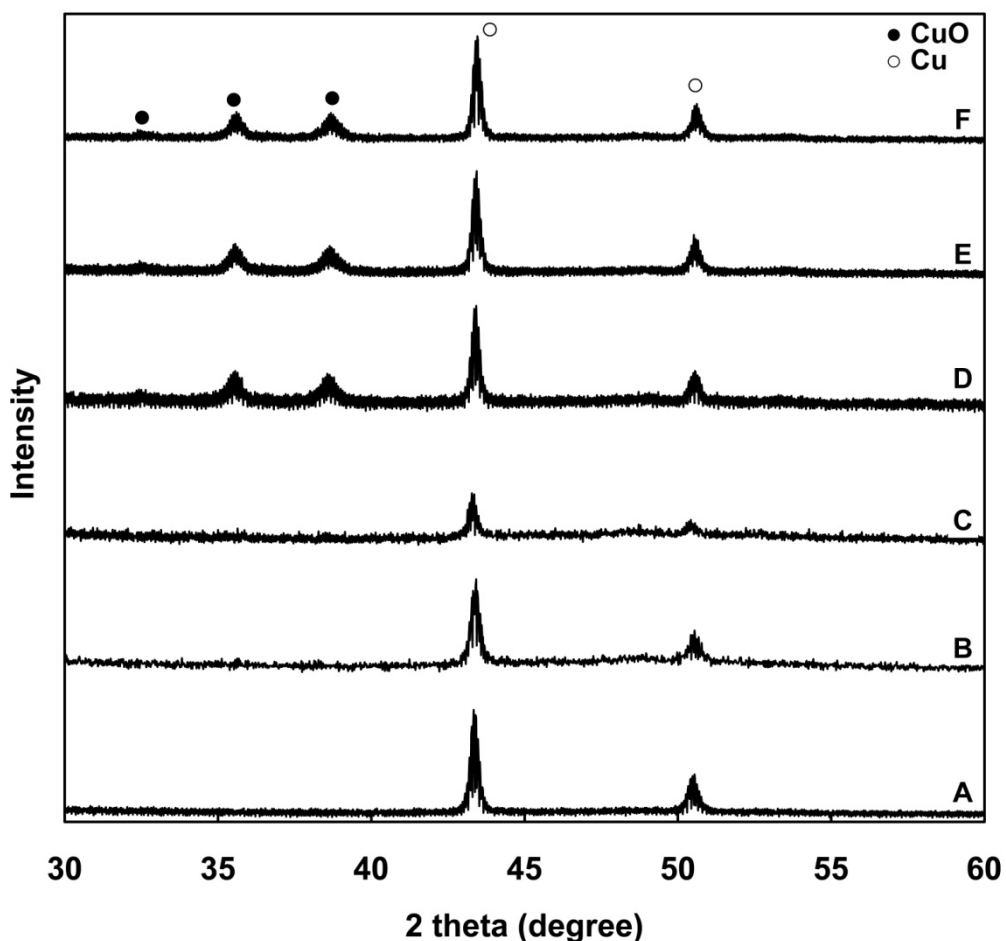


Fig. S6 XRD patterns of CuO nanobelts obtained at varied reaction periods: (A), 10min; (B), 30min; (C), 1h; (D), 3h; (E), 7h; (F), 10h. 100 mM NH₃–100 mM H₂O₂ aqueous solution (19 mL); reaction temperature, 80 °C.

Fig. S7

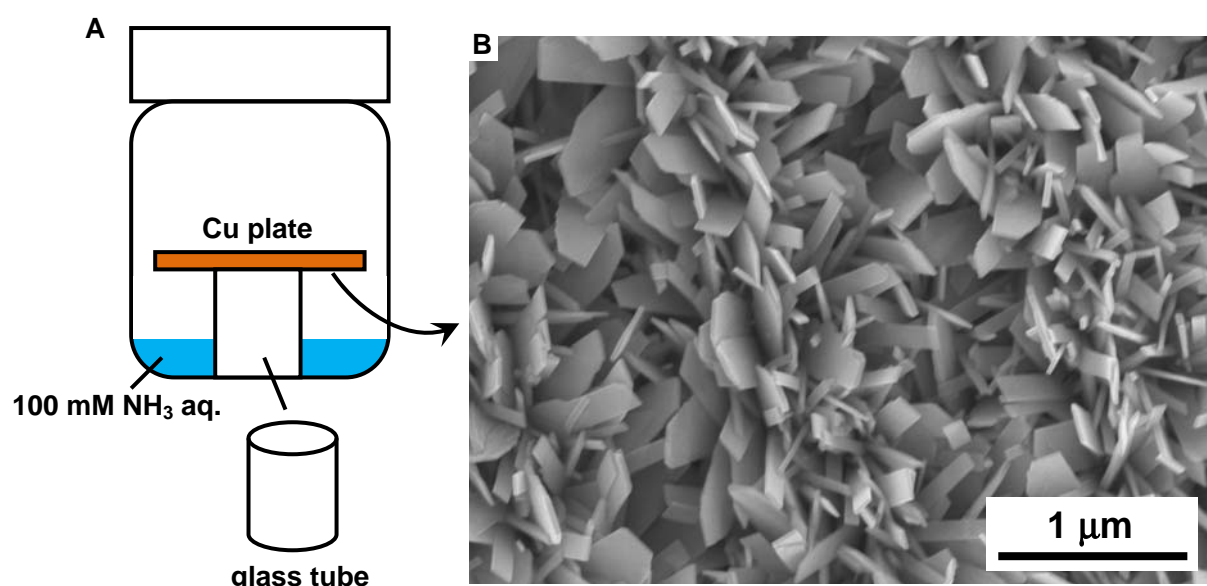


Fig. S7 (A) A schematic illustration of a VO process. (B) An SEM image of Cu nanobelt arrays formed by the vapor oxidation process.

Fig. S8

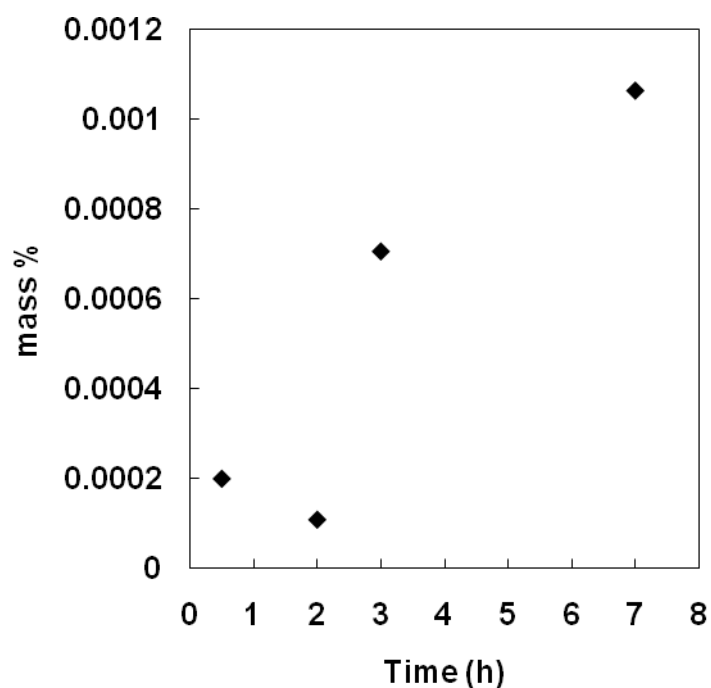


Fig. S8 Time courses of the amount of copper in the $\text{NH}_3/\text{H}_2\text{O}_2$ aqueous solution after the VO reaction.

Fig. S9

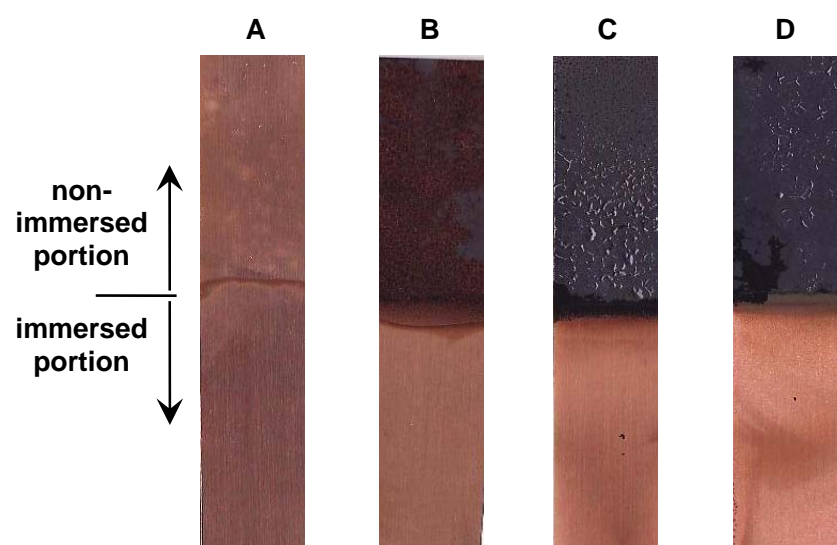


Fig. S9 Pictures of Cu substrates after the VO reaction: (A), 10min; (B), 1h; (C), 5h; (D), 24h. 100 mM NH₃ aqueous solution (19 mL); reaction temperature, 80 °C.

Fig. S10

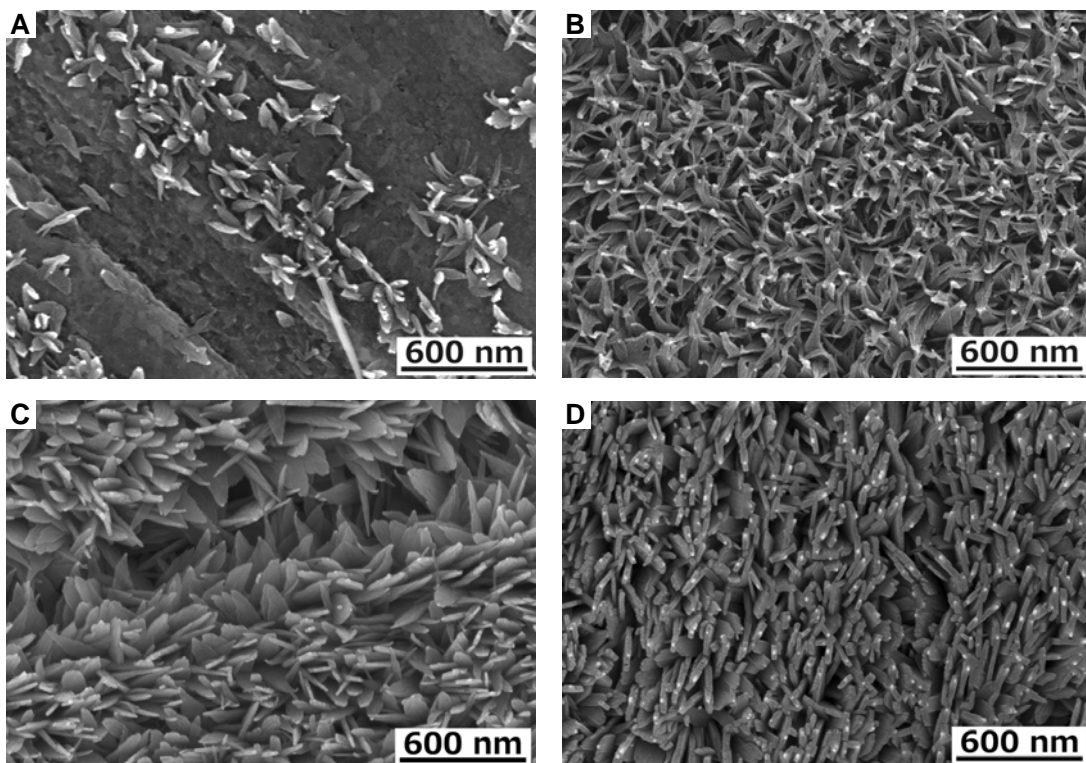


Fig. S10 SEM images of CuO nanobelt arrays obtained at varied reaction periods: (A), 10min; (B), 1h; (C), 5h; (D), 24h. 100 mM NH₃ aqueous solution (19 mL); reaction temperature, 80 °C.

Fig. S11

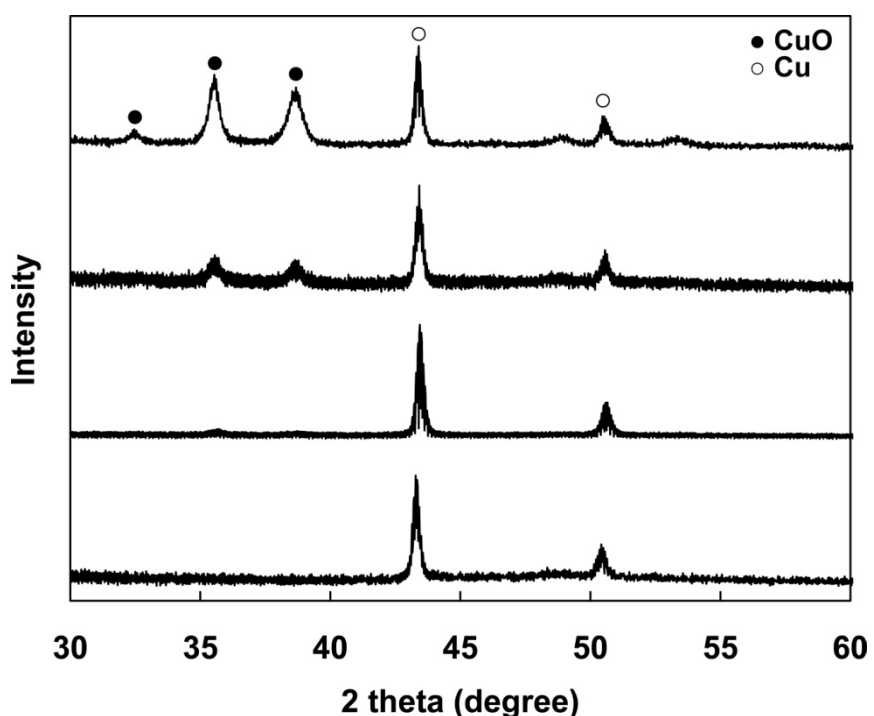


Fig. S11 XRD patterns of CuO nanobelt arrays obtained at varied reaction periods: (A), 10min; (B), 1h; (C), 5h; (D), 24h. 100 mM NH₃ aqueous solution (19 mL); reaction temperature, 80 °C.

Fig. S12

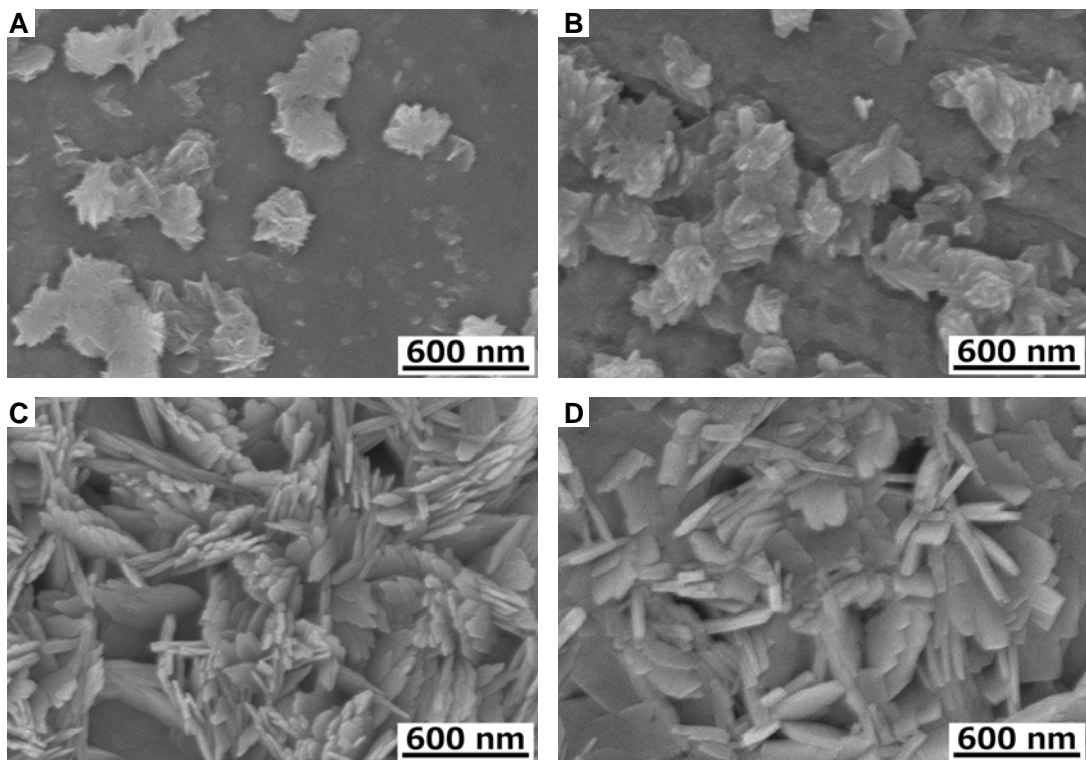


Fig. S12 SEM images of Cu plate after the VO reaction at varied pH: (A), pH 2; (B), pH 8; (C), pH 10; (D), pH 13.

100 mM NH₃ aqueous solution (19 mL); reaction temperature, 80 °C.

Fig. S13

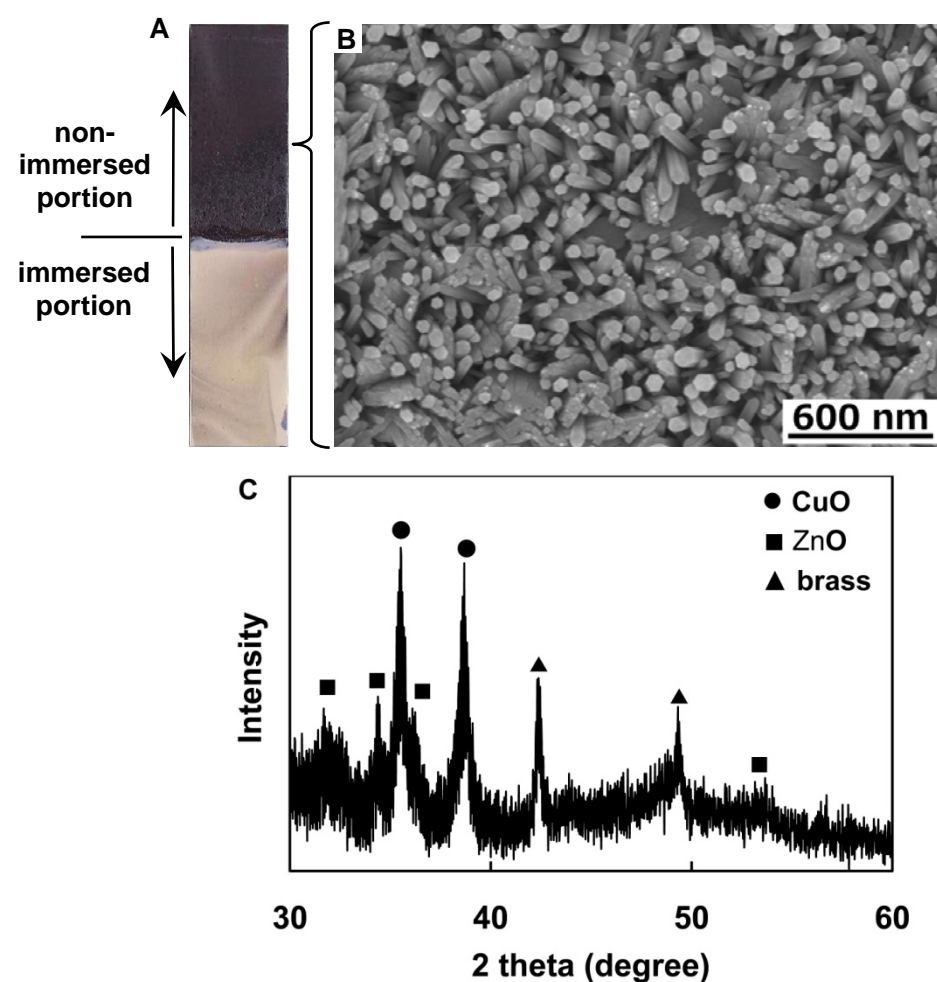


Fig. S13 (A) A Picture of a brass plate after the VO reaction (100 mM NH₃ aqueous solution, 24 h). A SEM image (B) and XRD pattern (C) of CuO/ZnO composite nanoarrays formed on brass plate.

Fig. S14

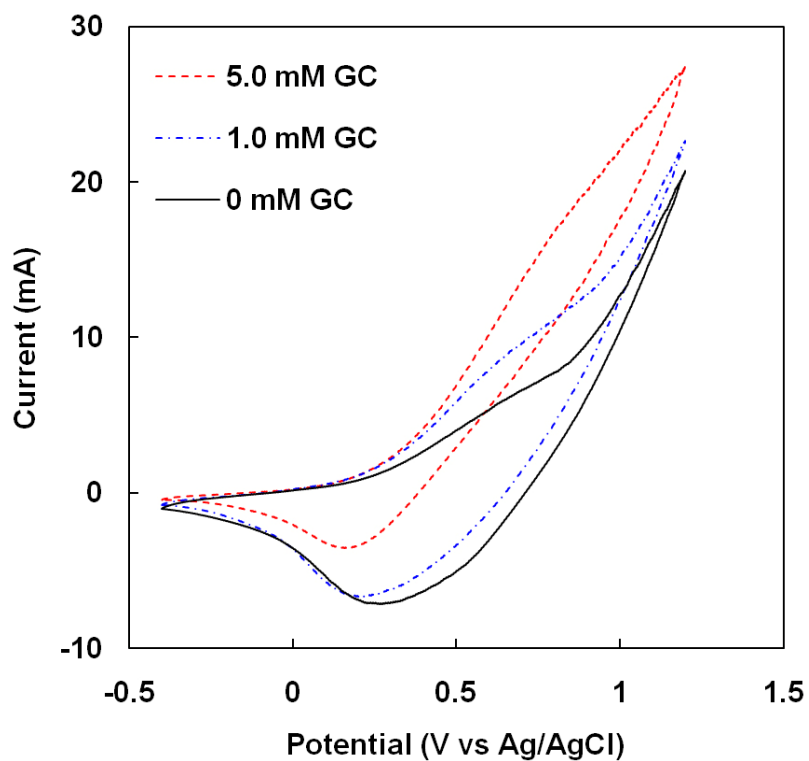


Fig. S14 Cyclic voltammograms (CVs) of glucose in 0.5 mol L⁻¹ NaOH. The scan rate is 10 mV s⁻¹.

Table S1

Table S1. Comparison of analytical performance of the present CuO nanobelt/Cu sensor with other reported non-enzymatic glucose sensors

Electrode type	Sensitivity ($\mu\text{A mM}^{-1}$ or $\mu\text{A mM}^{-1}\text{cm}^{-2}$)	Detection limit (μM)
Pt nanotube array electrode ¹	0.1	1.0
Mesoporous Pt electrode ²	9.6	N/A
Electrode based on bimetallic PtM (M = Ru, Pd, and Au)-CNT-ionic liquid ³	10.7	50.0
Porous Au electrode ⁴	11.8	5.0
Pt-Pb nanoparticles deposited on MWCNTs ⁵	17.8	1.8
Macroporous Pt electrode ⁶	31.3	0.1
3-D gold film electrode ⁷	46.6	3.2
Gold nanoparticles electrode ⁸	179.0	0.05
Cu nanocluster/MWCNTs/GC electrode ⁹	253.0	0.21
Gold nanowire array electrode ¹⁰	309.0	50.0
CuO nanorods-graphite electrode ¹¹	371.4	4.0
CuO nanospheres electrode ¹²	404.5	1.0
Ni-carbon nanofiber paste electrode ¹³	420.4	1.0
CuO nanofiber electrode ¹⁴	431.3	0.8
CuO nanowire modified Cu electrode ¹⁵	490.0	0.049
CuO nanowalls/Cu electrode ¹⁶	556.3	0.05
CuO nanobelts/Cu electrode (This work)	582.0	<1.0
Self-assembled CNT thin films with Cu nanoparticles electrode ¹⁷	602.0	0.1
CuO nanoflowers-graphite electrode ¹¹	709.5	4.0
Ni nanowire array electrode ¹⁸	1043	0.1
CuxO nanoflower/Cu electrode ¹⁹	1620	0.049
CuO-MWCNTs array electrode ²⁰	2190	0.8

References

1. J. H. Yuan, K. Wang, X. H. Xia, *Adv. Funct. Mater.*, 2005, **15**, 803-809.
2. S. Park, T. D. Chung, H. C. Kim, *Anal. Chem.*, 2003, **75**, 3046-3049.
3. F. Xiao, F. Q. Zhao, D. P. Mei, Z. R. Mo, B. Z. Zeng, *Biosens. Bioelectron.*, 2009, **24**, 3481-3486.
4. Y. Li, Y. Y. Song, C. Yang, X. H. Xia, *Electrochim. Commun.*, 2007, **9**, 981-988.
5. H. F. Cui, J. S. Ye, W. D. Zhang, C. M. Li, J. H. T. Luong, F. S. Sheu, *Anal. Chim. Acta*, 2007, **594**, 175-183.

6. Y. Y. Song, D. Zhang, W. Gao, X. H. Xia, *Chem. Eur. J.*, 2005, **11**, 2177-2182.
7. Y. Bai, W. W. Yang, Y. Sun, C. Q. Sun, *Sens. Actuators B*, 2008, **134**, 471-476.
8. B. K. Jena, C. R. Raj, *Chem. Eur. J.*, 2006, **12**, 2702-2708.
9. X. H. Kang, Z. B. Mai, X. Y. Zou, P. X. Cai, J. Y. Mo, *Anal. Biochem.*, 2007, **363**, 143-150.
10. S. Cherevko, C. H. Chung, *Sens. Actuators B*, 2009, **142**, 216-223.
11. X. Wang, C. Hu, H. Liu, G. Du, X. He, Y. Xi, *Sens. Actuators B*, 2009, **144**, p. 220-225.
12. E. Reitz, W. Z. Jia, M. Gentile, Y. Wang, Y. Lei, *Electroanalysis*, 2008, **20**, 2482-2486.
13. Y. Liu, H. Teng, H. Q. Hou, T. Y. You, *Biosens. Bioelectron.*, 2009, **24**, 3329-3334.
14. W. Wang, L. Zhang, S. Tong, X. Li, W. Song, *Biosens. Bioelectron.*, 2009, **25**, 708-714.
15. Z. Zhuang, X. Su, H. Yuan, Q. Sun, D. Xiao, M. M. F. Choi, *Analyst*, 2008, **133**, 126-132.
16. Z. Zhang, A. Gu, G. Wang, Y. Wei, W. Wang, H. Wu, B. Fang, *CrystEngComm*, 2010, **12**, 1120-1126.
17. X. Li, Q. Y. Zhu, S. F. Tong, W. Wang, W. B. Song, *Sens. Actuators B*, 2009, **136**, 444-450.
18. L. M. Lu, L. Zhang, F. L. Qu, H. X. Lu, X. B. Zhang, Z. S. Wu, S. Y. Huan, Q. A. Wang, G. L. Shen, R. Q. Yu, *Biosens. Bioelectron.*, 2009, **25**, 218-223.
19. C. Li, Y. Su, S. Zhang, X. Lv, H. Xia, Y. Wang, *Biosens. Bioelectron.*, 2010, **26**, 903-907.
20. J. Yanga, L.-C. Jiang, W.-D. Zhang, S. Gunasekaran, *Talanta*, 2010, **82**, 25-33.